

# Influence of azimuthal instabilities on electron motion in a Hall Effect Thruster

IEPC-2007-124

Presented at the 30<sup>th</sup> International Electric Propulsion Conference, Florence, Italy  
September 17-20, 2007

J. Pérez-Luna<sup>\*</sup>, G.J.M. Hagelaar<sup>†</sup>, L. Garrigues<sup>‡</sup>, N. Dubuit<sup>§</sup> and J.P. Boeuf<sup>\*\*</sup>  
*Laboratoire PLAsma et Conversion d'Énergie, LAPLACE*  
CNRS – Université Paul Sabatier, 118 Route de Narbonne, 31062 Toulouse cedex 9, France

Since the beginning of Hall Effect thrusters (HET) research, anomalous electron conductivity has been an outstanding question, preventing the development of predictive thruster models. The increasing interest in this technology for space exploration encourages further attempts to clarify this aspect of the thruster physics. The possible contribution of “near-wall conductivity” to the overall electron conductivity has been long discussed, but it now seems clear that anomalous conductivity due to plasma turbulence must be present to explain the experimental results. Recent PIC simulations have shown that azimuthal instabilities can lead to axial electron transport. In this paper, a simplified study of the influence of an azimuthal instability on electron transport is carried out in the case of a PPS1350 thruster. Adding a fluctuating azimuthal electric field to the time averaged field in the (r, z) plane given by a hybrid model, we have studied single electron trajectories from the cathode to the anode and deduced macroscopic electron transport properties. Our results show how electrons can be driven by the instability from the cathode to the anode and provide an estimate of the mean axial speed of the electrons in the discharge channel. Different amplitudes and wave numbers of the monomode azimuthal instability have been investigated.

## Nomenclature

$\mathbf{E}$	=	electric field vector
$\mathbf{B}$	=	magnetic field vector
$\nu_m$	=	total momentum-transfer rate frequency
$\nu_c$	=	classical momentum-transfer rate frequency
$\nu_b$	=	anomalous Bohm frequency
$\omega$	=	cyclotron frequency
$K$	=	empirical fitting parameter
$x, y, z$	=	cartesian coordinates
$x, r, \theta$	=	cylindrical coordinates
$E_x, E_r, E_\theta$	=	total electric field components
$E_{x, hybrid}, E_{r, hybrid}$	=	electric field components deduced from hybrid model
$B_x, B_r, B_\theta$	=	magnetic field components

---

<sup>\*</sup> PhD. student, perezluna@laplace.univ-tlse.fr

<sup>†</sup> Research scientist, hagelaar@laplace.univ-tlse.fr

<sup>‡</sup> Research scientist, garrigues@laplace.univ-tlse.fr

<sup>§</sup> Postdoctoral research associate, Dubuit@laplace.univ-tlse.fr

<sup>\*\*</sup> Senior scientist, jpb@laplace.univ-tlse.fr

$E_0$	=	maximum electric field in domain
$\lambda$	=	lambda stream function, related to magnetic field
$\alpha$	=	maximum instability amplitude
$k_\theta$	=	wave number
$f$	=	instability amplitude distribution function
$V_{tot}$	=	total electric potential
$V'$	=	perturbation on electric potential
$V_{hybrid}$	=	electric potential deduced from hybrid model
$T_e$	=	electron temperature
$\Delta t$	=	time step
$v_1, v_f, v_2$	=	intermediate speeds
$v_t$	=	electron speed at t
$\mathbf{x}_t$	=	electron position at t
$\tau$	=	electron transit time from cathode to anode

## I. Introduction

Hall Effect thrusters are one of the most promising electric propulsion devices for the future, especially after the success of the European lunar probe SMART-1<sup>1</sup>. These devices have been used and studied since the late sixties and many thrusters have been successfully used in station keeping and orbit transfer missions. Despite this, the physics involved is still not fully mastered. Even though the general concept is well understood, several major questions have no answer. One of them is the question of anomalous electron transport across the magnetic field. The measured current in HETs is larger than can be estimated assuming classical (i.e. due to collisions with neutral atoms) electron conductivity. Recent HET modeling efforts have been limited by this lack of understanding of anomalous electron transport, and the models are not fully predictive.

Several theories on anomalous conductivity have been proposed but none is fully convincing. These theories can be separated into two groups: electron-wall interactions and plasma turbulence. Morozov was the first to take into consideration electron-wall interactions with the so-called “near-wall conductivity” in an attempt to explain the large axial conductivity observed experimentally<sup>2</sup>. He suggested that electron wall scattering was related to specular reflection of electrons on the wall sheath, assuming that the sheath is thin enough to follow the roughness of the wall. During the renewed interest in HET in the 1990s, Bugrova carried out an important experimental work on electron-wall interactions to investigate some of the predictions of Morozov’s theory referenced above<sup>3</sup>. One of the main conclusions was the correlation between the roughness of the channel walls and the discharge current. Nevertheless, real channel roughness does not seem sufficient to explain experimental currents. More recently, authors have stressed the role of secondary electron emission (SEE) at the walls<sup>4,5,6,7</sup>. The physics of these electron-wall interactions is still uncertain, and authors do not always agree on correlations between these interactions and electron cross-field transport or electron temperature saturation. Recently, Garrigues *et al.*<sup>8</sup> have shown that even if SEE can account for electron energy losses it seems that it is not sufficient to explain cross-field electron transport. Finally, electron-wall interactions may play a role in the discharge channel but the role of the walls outside the channel, i.e. between the cathode and the channel entrance is questionable.

The other theory invoked by several authors is microturbulence and electric field turbulence. Many authors<sup>9,10,11</sup> include in their models an anomalous Bohm conductivity to account for microturbulence in the plasma. This anomalous conductivity is often adjusted by different means to obtain simulation results in agreement with experimental results. One of the first experimental results concerning field turbulence in a HET-like device was published by Janes and Lowder<sup>12</sup>. They evidenced the correlation between a rotating electron density bulk in the direction of  $\mathbf{E} \times \mathbf{B}$  and resulting azimuthal electric fields. Literature concerning azimuthal behavior in HET is scarce compared to radial and axial studies. Most of models use an axial or axial and radial geometry. But more and more authors show interest in azimuthal phenomena in the thruster. Recently, many experimental characterizations of turbulence in HET have been carried out and emphasize the importance of plasma turbulence in anomalous conductivity<sup>13,14,15</sup>. Adam *et al.*<sup>16</sup> have undergone a two dimensional fully PIC model of a HET in the axial and azimuthal directions. They have revealed the existence of a rotating electric azimuthal field wave, just as Janes and Lowder did experimentally. They have also showed the correlation between this wave and anomalous electron transport.

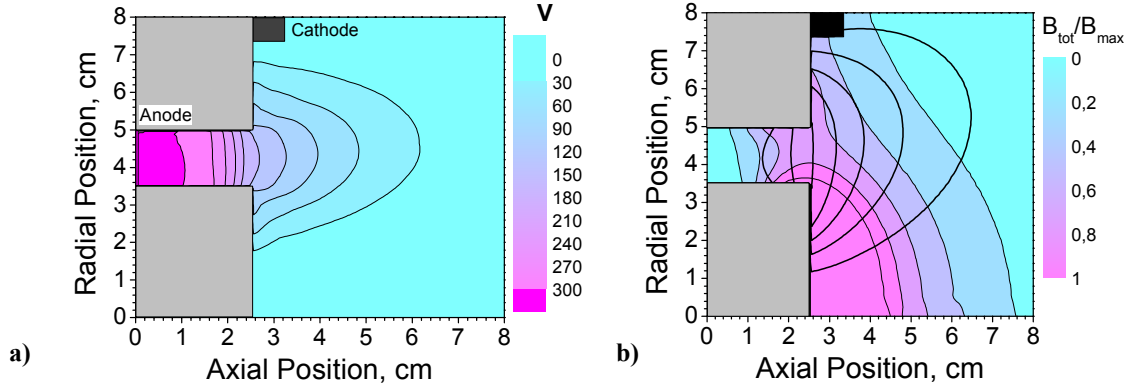


**Figure 1: (a) Electric potential, and (b), magnetic field amplitude (normalized) and contours as calculated with our hybrid model for an SPT100 in nominal configuration: mass flow rate  $5 \text{ mg}\cdot\text{s}^{-1}$  and voltage drop 300V.**

We have developed during the past years a 2D (radial and axial directions) hybrid model of a HET<sup>17</sup>. In this model anomalous electron transport is taken into account using effective collision frequencies associated with Bohm diffusion and electron-wall interaction. These transport coefficients involving the effective collision frequency are adjusted to match experimental data<sup>10</sup>. The model is therefore not self-consistent and, in order to improve the hybrid model, it is necessary to find scaling laws for the anomalous transport coefficients.

The aim of the present work is to study the influence of an azimuthal electric field wave on collisionless electron transport between cathode and anode in a real thruster configuration. The electron trajectories are computed using electric and magnetic fields obtained with the hybrid code, and superimposing an azimuthal electric field wave. This study is therefore not self-consistent (the azimuthal field wave is given), but can provide useful information, in parallel with more complete (and much more time consuming) PIC simulation results.

Section II presents the results used from the hybrid code and the choice and definition of the azimuthal instability. In Section III, we describe the particle model used for the electrons. Section IV presents results obtained for different field waves.

## II. Inputs from hybrid code and azimuthal instability

We have simulated the trajectories of electrons injected at the cathode location. To do this, we need to know the electric and magnetic fields in the simulation domain, which includes the discharge channel and the near-field area of the thruster. These field distributions are deduced from our hybrid model results. This model is a 2D quasineutral model in the radial and axial directions. Ions and neutral atoms are described by particle simulations. Electrons are described by fluid equations. The model has recently been updated with a new algorithm that allows the use of the same fully 2D grid for the electron fluid equations and the particle computation<sup>18</sup>. In order to take into account the anomalous electron mobility, the model adds to the classical momentum-transfer rate frequency ( $\nu_c$ ) and anomalous Bohm frequency ( $\nu_b$ ):

$$\nu_m = \nu_c + \nu_b = \nu_c + \frac{K\omega}{16} \quad (1)$$

where  $\omega$  is the cyclotron frequency and  $K$  is set to fit experimental results. Simulation results using adequate  $K$  coefficients yield a convenient 2D potential distribution for a given thruster configuration. Magnetic field is computed using the finite element magnetic solver FEMM<sup>19</sup>. Both fields are calculated on the same 2D grid. Azimuthal symmetry for the electric potential and magnetic field is assumed. Figure 1 shows the electric potential and the magnetic field for an SPT100 thruster<sup>20</sup> in its nominal configuration: 300V potential drop between the cathode and the anode and a xenon mass flow rate of  $5 \text{ mg}\cdot\text{s}^{-1}$ . The results presented later were all obtained in this configuration.

As mentioned in the introduction, Adam *et al.*<sup>16</sup> have shown the existence of an azimuthal instability in a cross-field thruster type configuration using a particle-in-cell model in the azimuthal and axial directions.

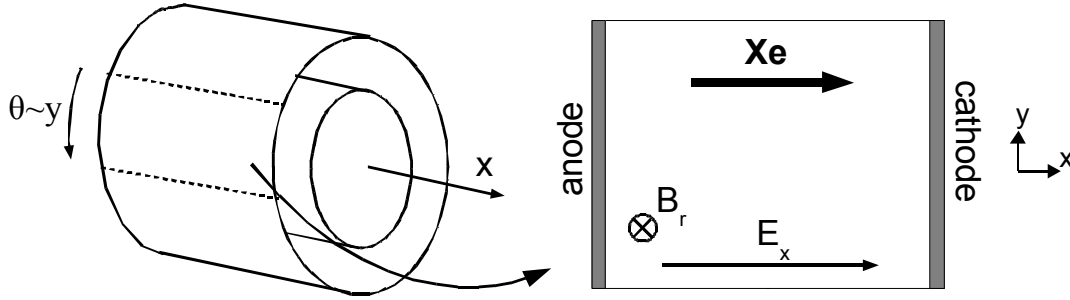


**Figure 2: PIC model geometry and boundaries, the magnetic field is purely radial and the electric field axial.**

Figure 2 shows the geometry and boundary conditions of the model of Adam *et al.*. This particle-in-cell model has essentially no free parameters: the authors use a true mass ratio of ionized xenon to electron, and ionization and electron-neutral collision have the energy dependence found in standard tables. The geometry is in the axial and azimuthal directions and secondary emission and wall recombination are neglected. Their results show the development of plasma turbulence driven by the electron drift. The PIC simulations results are in good agreement with experiments, without including diffusive electron wall collisions.

The plasma turbulence in the azimuthal direction in the PIC simulations of Adam *et al.* is visible in Fig. 3. We show here the amplitude of the azimuthal component of the electric field for a 300V potential drop between the cathode and the anode and a  $5\text{mg}\cdot\text{s}^{-1}$  mass flow rate. We clearly see the existence of an oblique wave. The wave length is of a few  $10^{-4}$  m, which corresponds to a wave number of  $k_y=10^4\text{ m}^{-1}$  or  $k_\theta\sim 4\cdot 10^2\text{ rad}^{-1}$  if the mean radius is  $4\cdot 10^{-2}\text{ m}$  ( $k_\theta=k_y/r$ ). An exhaustive work on this instability can be found in the paper by Ducrocq *et al.*<sup>21</sup>.

In the present work, we assume a given form of the azimuthal field perturbation described by Ducrocq *et al.*. From the work of these authors, one can define a simple form of this field as follows:

$$E_\theta(x, r, \theta) = \alpha f(\lambda) E_0 \cos(k_\theta \theta) \quad (2)$$

where  $x$  is the axial position (zero at anode),  $r$  the radial position (zero at thruster axis),  $\theta$  the azimuth,  $k_\theta$  is the wave number,  $\alpha$  a multiplication coefficient ( $0 < \alpha < 1$ ) and  $E_0$  the maximum electric field in the whole domain.  $f(\lambda)$  is a function of lambda, where  $\lambda$  is a stream function constant along the magnetic field lines and is defined as:

$$B_x = -\frac{1}{r} \frac{\partial \lambda}{\partial r} \quad B_r = \frac{1}{r} \frac{\partial \lambda}{\partial x} \quad (3)$$

Function  $f$  is used to control precisely the amplitude of the perturbation. In the simplified configuration of Fig. 2 (radial magnetic field and axial electric field), the azimuthal instability is located around the acceleration area, where the  $\mathbf{E} \times \mathbf{B}$  drift is strongest. In the more complex configuration generated with our hybrid code, the  $\mathbf{E} \times \mathbf{B}$  drift is still strong outside the channel, around the exit plane.  $f$  is chosen so that the amplitude of the perturbation is maximum in the acceleration region but decreases near the anode and outside the channel. Figure 4 shows the chosen function  $f$ .

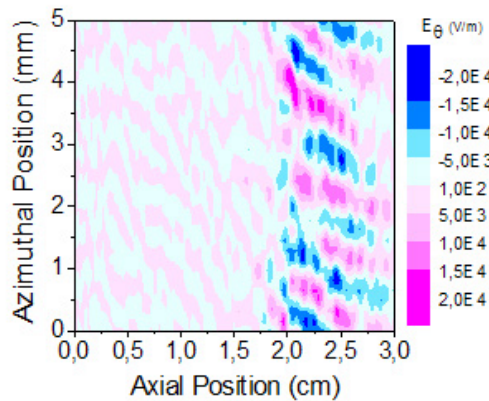


**Figure 3: Azimuthal component of the electric field (V/m) as evidenced by Adam *et al.*<sup>16</sup>**

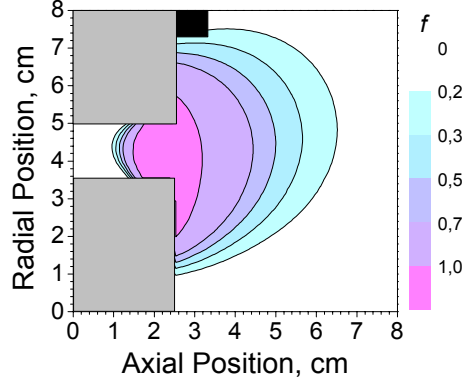


**Figure 4: Function  $f$  which defines the amplitude of the potential perturbation in the  $(x,r)$  plane.**

The choice can seem arbitrary. It is actually impossible to determine exactly where the instability should be effective because we have no information on the exterior of the discharge channel. We believe our choice is consistent with the PIC results. The maximum amplitude of the perturbation  $\alpha$  and the wave number  $k_\theta$  are the main parameters used to change the azimuthal perturbation.  $f$  is not changed.

We have just defined the azimuthal perturbation as an electric field wave. Nevertheless, if we add such a perturbation to the electric field determined with the hybrid model, the electric potential and the electric field will not be consistent because adding only an azimuthal component to the electric field leads to an electric field which does not derive from a potential. To avoid this, we introduce a perturbation on the potential itself defined as:

$$V'(x,r,\theta) = \frac{\alpha f(\lambda) r E_0}{k_\theta} \sin(k_\theta \theta) \quad (4)$$

The total potential reads then:

$$V_{tot}(x,r,\theta) = V_{hybrid}(x,r) + V'(x,r,\theta) \quad (5)$$

The resulting electric field becomes:

$$E_x = -\frac{\partial V_{tot}}{\partial x} = -\frac{\partial V_{hybrid}(x,r)}{\partial x} - \frac{\partial V'(x,r,\theta)}{\partial x} = -E_{x,hybrid} - \frac{\alpha r E_0}{k_\theta} \frac{\partial f(\lambda)}{\partial x} \sin(k_\theta \theta) \quad (7)$$

$$E_r = -\frac{\partial V_{tot}}{\partial r} = -\frac{\partial V_{hybrid}(x,r)}{\partial r} - \frac{\partial V'(x,r,\theta)}{\partial r} = -E_{r,hybrid} - \frac{\alpha r E_0}{k_\theta} \frac{\partial f(\lambda)}{\partial r} \sin(k_\theta \theta) \quad (8)$$

$$E_\theta = -\frac{1}{r} \frac{\partial V_{tot}}{\partial \theta} = -\frac{1}{r} \left( \frac{\partial V_{hybrid}(x,r)}{\partial \theta} - \frac{\partial V'(x,r,\theta)}{\partial \theta} \right) = \alpha f(\lambda) E_0 \cos(k_\theta \theta) \quad (9)$$

where  $E_i$  are the components of the total electric field,  $E_{x,hybrid}$  is the axial component of the electric field of the hybrid model,  $E_{r,hybrid}$  the radial component of the electric field of the hybrid model,  $V_{tot}$  the total electric potential,  $V_{hybrid}$  the potential from the hybrid model and  $V'$  the potential perturbation. This way, we obtain the desired azimuthal electric field wave and avoid any ensure energy conservation.

### III. Electron motion computation

The electron trajectories are studied in a 3D geometry. The domain includes the discharge channel and an exterior cylinder of 8cm in length in the axial direction starting from the anode and a 8cm radius, so that it encloses the cathode. Electrons are emitted from a point at  $x=2.6\text{cm}$  and  $r=7\text{cm}$ , which corresponds to the cathode position

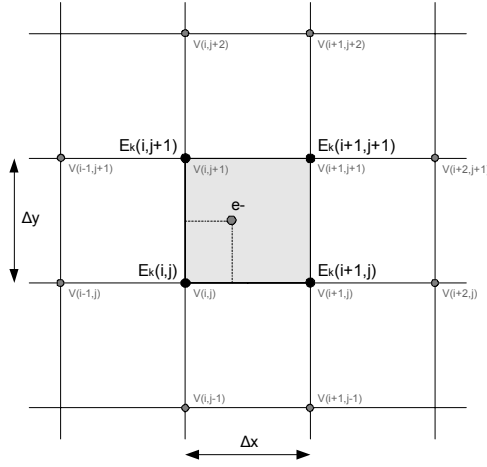


**Figure 5: Inclusion of the potential perturbation and interpolation of the fields in the active cell**

for a PPS1350 thruster. Their initial speed is determined by a Maxwellian distribution flux tilted 45 degrees towards the centre of the thruster and with  $T_e=5\text{eV}$  for the initial electron temperature. When an electron exits the computation domain, a new one is emitted at the same initial position. We have studied single trajectories as well as statistical data. The electron equations of motion are computed using a typical explicit leap-frog scheme and the implementation of the  $\mathbf{v} \times \mathbf{B}$  rotation due to the  $\mathbf{E} \times \mathbf{B}$  cross field is the one described by Boris<sup>22</sup>:

$$\begin{aligned}
 \mathbf{v}_1 &= \mathbf{v}_{t-\frac{\Delta t}{2}} + \frac{q\Delta t}{2m} \mathbf{E} \\
 \mathbf{v}_f &= \mathbf{v}_1 + \mathbf{v}_1 \times \frac{\omega\Delta t}{2} \mathbf{b} \\
 \mathbf{v}_2 &= \mathbf{v}_1 + \mathbf{v}_f \times \frac{2t}{1+t^2} \mathbf{b} \\
 \mathbf{v}_{t+\frac{\Delta t}{2}} &= \mathbf{v}_2 + \frac{q\Delta t}{2m} \mathbf{E} \\
 \mathbf{x}_{t+\Delta t} &= \mathbf{x}_t + \mathbf{v}_{t+\frac{\Delta t}{2}} \Delta t
 \end{aligned} \tag{10}$$

where  $\Delta t$  is the time step,  $\mathbf{v}_1$ ,  $\mathbf{v}_f$ ,  $\mathbf{v}_2$  intermediate speeds,  $\mathbf{v}_t$  the particle speed and  $\mathbf{x}_t$  its position.  $\mathbf{b}$  is an unitary vector in the direction of  $\mathbf{B}$ . Elastic collisions are taken into account in our model. The collision frequency is obtained from the hybrid model. Ionization and inelastic collisions are not taken into account. There are no energy losses. Wall reflection is specular.

We have already presented the input fields from the hybrid code and how we chose the perturbation on the electric potential. We now briefly expose the inclusion of the perturbation calculation in the interpolation of the electric field. The perturbation is added to the potential so we preferred to use an energy conserving scheme to interpolate the electric field<sup>23</sup>. We obtain the electric potential on each nod using the hybrid model and then calculate on each nod the corresponding electric field using the finite differences technique. This allows us to define the potential perturbation on each nod using Eq. 4, which we add to the potential from the hybrid model. The total potential is then interpolated bilinearly in the active cell. We finally derive the electric potential to know the total electric field at the particle position. For the magnetic field, we know the lambda function, defined previously.  $\lambda$  is known on each nod. It is interpolated and the magnetic field is calculated using Eq. 3.

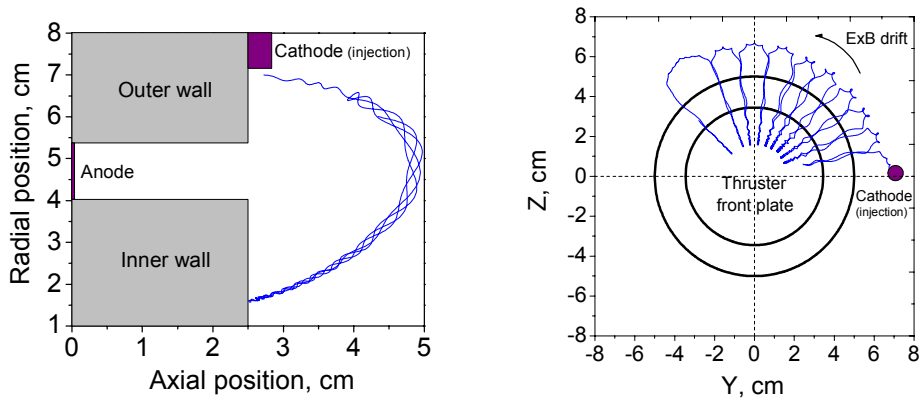


Figure 6: Electron trajectories in the discharge channel of an SPT100 in nominal configuration ( $V_d=300V$  and  $\dot{m}=5\text{ mg}\cdot\text{s}^{-1}$ ) – half-side view (a) and front view (b).

#### IV. Simulation results

##### A. Electron trajectories

If an electron is placed in the cross-field configuration of a HET, it will remain trapped along the same magnetic field line and turn around the thruster axis with an  $E \times B$  drift. This is what we see on Fig. 6 with two different planar views: a front view of the thruster and a half side view. Field gradients can be responsible for electron drift but not in the axial direction<sup>24</sup>. Collisions do change the magnetic field line around which the electron is trapped. The axial electric field due to the potential drop combined with collisions transports the electron towards the anode. Electron axial mobility quantifies this axial drift. Nevertheless, we have already explained that the theoretical electron mobility due to collisions with neutral atoms near the channel exit and outside the channel is too low to explain the experimental currents. We study in this section the anomalous electron transport in the cross-field configuration of the SPT100 associated with an azimuthal perturbation of the potential as defined above.

Figure 7 shows two electron trajectories. In both cases, the same electric and magnetic field distribution was used and no collisions were introduced. The electron was injected at the same point with the same initial energy (5eV). The trajectory on the left was obtained with no perturbation. The one on the right was obtained by adding an azimuthal perturbation as described earlier, and by choosing  $\alpha=1$  and  $k^{\theta}=4.10^2\text{ rad}^{-1}$ .  $\alpha$  is voluntarily chosen high to illustrate the effect of the perturbation. We will see later the influence of  $\alpha$ . The meaning of  $k_{\theta}$  has been defined

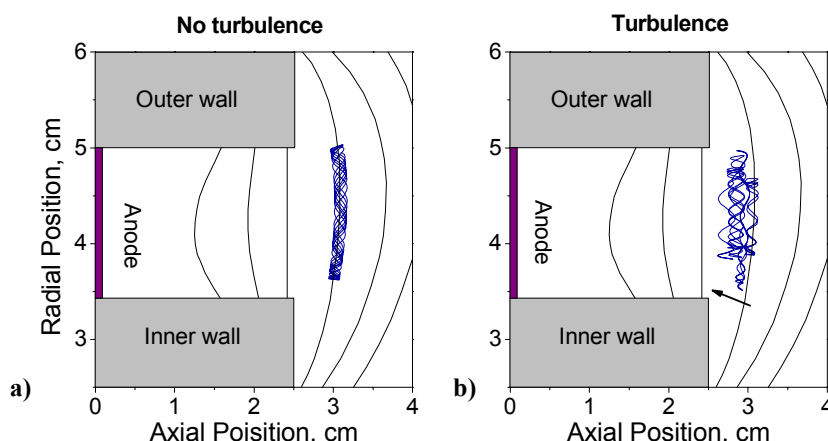


Figure 7: Electron trajectories in the discharge channel of an SPT100 in nominal configuration ( $V_d=300V$  and  $\dot{m}=5\text{ mg}\cdot\text{s}^{-1}$ ) with (b) and without turbulence (a).

**Table 1: Mean transit time  $\tau$  from cathode to anode for different amplitudes ( $\alpha$ ) and wave numbers ( $k_0$ ).**

$k_0$ (rad <sup>-1</sup> )	$\alpha$	$\tau$ (s)
4.10	0.2	$3,95 \cdot 10^{-5}$
$10^2$	0.2	$4,95 \cdot 10^{-5}$
$4 \cdot 10^2$	0.2	$8,32 \cdot 10^{-5}$
$10^3$	0.2	$1,09 \cdot 10^{-4}$
$4 \cdot 10^2$	0.1	$1,35 \cdot 10^{-4}$
$4 \cdot 10^2$	0.5	$3,38 \cdot 10^{-5}$
$4 \cdot 10^2$	1	$1,68 \cdot 10^{-5}$

previously and a parametric study of the wave number is also presented below. We see that the electron drifts towards the interior of the discharge channel because of the perturbation. A longer simulation time would show that the electron eventually enters the discharge channel. The field perturbation has the same effect as collisions and changes the magnetic field line around which the electron is trapped. As explained in section II, the perturbation is only applied in a selected area (by using function  $f$ ). The influence of the turbulence on the electron trajectory exists in this same area. If collisions are added to the simulation, an electron injected at the cathode can reach the anode. Total energy conservation is checked for each computed trajectory to avoid numerical heating (the criteria is that the numerical heating must be  $<2\%$  of the electron energy). In general, this condition is satisfied for  $\Delta t = 10^{-11}$  s, which is our standard value for the integration time step.

### B. Macroscopic effects

After the study of single electron trajectories, we proceeded to a statistical study to characterize the effect of different azimuthal perturbations. Electrons were all injected one by one at the cathode with a Maxwellian flux distribution with an initial electron temperature of  $T_e = 5$  eV. Collisions are taken into account and the collision frequency is deduced from our hybrid model results (collisions are sufficient to provide transport close to the anode, because of the relatively large neutral density, but are not sufficient around the channel exit and outside the channel because of the neutral density drop due to ionization). Electric field, magnetic field, initial temperature conditions and position are the same for each electron. Each time an electron gets to the anode, a new electron is injected at the cathode. Two parametric studies were carried out. The first set of simulations was carried out with a fixed wave number ( $k_0 = 4 \cdot 10^2$  rad<sup>-1</sup>) and for different values of  $\alpha$  (0.1, 0.2, 0.5 and 1). The second one with a fixed  $\alpha = 0.2$  and different wave numbers ( $k_0 = 40, 10^2, 4 \cdot 10^2$  and  $10^3$  rad<sup>-1</sup>). The mean transit time  $\tau$  from the cathode to the anode is presented in table 1 for each case. The order of magnitude is of several  $10^{-5}$  s,  $10^{-4}$  s in the slower cases. The general trend is that the electrons cross faster the domain when the amplitude of the perturbation increases but also when the wave number decreases.

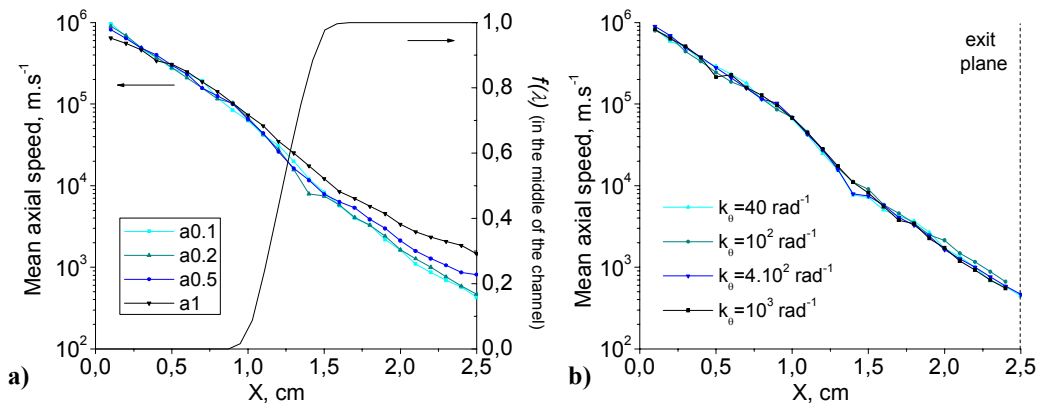


**Figure 8: electron axial mean speed along the thruster axis in the discharge channel of an SPT100 for different perturbation amplitudes (a) and wave lengths (b) – presented values are a statistic of 1000 electrons fired from the cathode. We also present the value of  $f$  in the middle of the channel (a).**

Figure 8 shows the mean axial speed of electrons in the discharge channel. Mean axial speed is calculated at each plane. The function  $f$  remains the same and its value in the middle of the channel is also detailed in Fig. 8. On the left are presented the simulation results for different amplitudes  $\alpha$  and a same wave number  $k_0=4.10^2 \text{ rad}^{-1}$ . On the right are presented the results for different wave numbers  $k_0$  and a same  $\alpha=0.2$ . In the first case, we see that the axial drift increases with the amplitude but that if  $\alpha$  is multiplied by a factor 10, the mean electron axial speed at the exit plane ( $x=2.5\text{cm}$ ) is only multiplied by a factor 3. An interesting result, which could be predicted considering the choice of function  $f$ , is that in the region close to the anode,  $\alpha$  has no influence on the results: in this region only collisions are responsible for the electron axial drift. It is interesting to see that even with a very low amplitude, the perturbation creates a considerable electron drift. In the second case, there is a lesser difference in the mean axial speeds for different wave numbers. This is surprising because table 1 shows that the transit time decreases when the wave number does. The only explanation we have is that the wave-electron interaction is different outside the channel because the region where the turbulence is applied is larger outside the channel (see Fig. 4). Also, the computation of the mean axial speed is far noisier than the calculation of the transit time.

On the whole, these results show how the potential perturbation produces an axial drift towards the anode. In our work we have only used a monochromatic, azimuthal wave to illustrate the plasma turbulence. Of course, the thruster surely presents multimode and oblique waves which are much more complex to study. We do not pretend to depict what happens precisely in the thruster but rather to explain what physical mechanisms can explain the entry of electrons in the discharge channel. Also, we know that, for a potential drop around 300 V, the mean velocity of the ions ejected from the channel should be on the order of  $10^4 \text{ m/s}$ . Because of flux conservation and plasma quasineutrality, the mean velocity of electrons entering the channel is on the same order as the velocity of ions at the same location. More precisely, since the electron current is about 1/3 of the ion current in the exhaust region, and because of quasineutrality, the electron velocity should be about 3 times less than the ion velocity. Therefore, the order of magnitude predicted by the simulations and associated with the azimuthal field perturbation taken into account in the calculations, is consistent with the expected value of the mean velocity.

## V. Conclusion

Since the beginning of HET, anomalous electron conductivity has prevented a full understanding of these thrusters and the development of fully predictive models. Anomalous electron transport is also one of the most controversial questions in HET theory. Experimental and modeling results have evidenced that turbulence can induce an electron axial transport.

In this paper we have simulated electron trajectories in a HET, for an  $(r, z)$  electric field distribution deduced from a hybrid model and superimposed with an azimuthal field perturbation as predicted by PIC simulations and analytical theories. The amplitude and wave number of the azimuthal field wave were used as parameters. The trajectory simulations confirm that such azimuthal wave can provide the necessary electron momentum changes that allow electron transport across the magnetic field in a real HET configuration. The calculations provide estimates of the wave parameters (amplitude and wave length) leading to electron mean velocities in the channel consistent with expected values. The calculated electron velocity is consistent with expected values when rather large values of the azimuthal wave amplitude (about 20% of the axial field) are chosen (this is consistent with PIC simulations). More work is needed to study electron transport in the presence of an azimuthal wave, and to try, with the help of PIC simulations and experiments (e.g. LIF measurements of the ion velocity distribution), to determine scaling laws for the azimuthal field wave.

## Acknowledgments

This work was performed in the frame of the Groupement De Recherche CNRS/CNES/ SNECMA/ Universities n°2759 "Propulsion Spatiale à Plasma" and the French ANR (National Research Agency, project TELIOPEH, ANR-06-BLAN-0171) . The authors would like to thank J.C. Adam and A. Heron for a number of helpful discussions, and for providing their database of PIC simulation results. J. Perez-Luna benefits from a CNES/SNECMA PhD fellowship. N. Dubuit benefits from an ANR post-doctoral fellowship.

## References

- <sup>1</sup> Koppel C.R., Marchandise F., Prioul M., Estublier D., Darnon F., "The SMART-1 electric propulsion subsystem around the Moon: In flight experience", *34<sup>th</sup> Joint Propulsion Conference and Exhibit*, Tucson, Arizona, paper AIAA 05-3671, 2005.
- <sup>2</sup> Morozov A. I., Savel'ev V.V., "Theory of the near-wall conductivity", *Plasma Phys. Rep.*, Vol. 27, No. 7, pp. 607-613, 2001.
- <sup>3</sup> Bugrova A. I., Desyatkov A. V., Morozov A. I., and Kharchenikov V. K., *Plasma Phys. Rep.*, Vol. 4, pp. 302, 1996.
- <sup>4</sup> Barral S., Makowski K., Peradynski Z., Gascon N., and Dudeck M., "Wall material effects in stationary plasma thrusters. II. Near-wall and in-wall conductivity", *Phys. Plasmas*, Vol. 10, No. 10, pp. 4137-4152, 2003.
- <sup>5</sup> Ahedo E. and Gallardo M., "Effects of the radial plasma-wall interaction on the Hall thruster discharge", *Phys. Plasmas*, Vol. 10, No.8, pp.3397-3409, 2003.
- <sup>6</sup> Raitses Y., Staack D., Smirnov A., and Fisch N. J., "Space charge saturated sheath regime and electron temperature saturation in Hall thrusters", *Phys. Plasmas*, Vol. 12, No. 073507, 2005.
- <sup>7</sup> Raitses Y., Smirnov A., Staack D., and Fisch N. J., "Measurements of secondary electron emission effects in the Hall thruster discharge", *Phys. Plasmas*, Vol. 13, No. 014502, 2006.
- <sup>8</sup> Garrigues L., Hagelaar G.J.M., Boniface C., and Boeuf J.P., "Anomalous conductivity and secondary electron emission in Hall effect thrusters", *J. Appl. Phys.*, Vol. 100, No.123301, 2006.
- <sup>9</sup> Fife J. M., Ph.D. Thesis, Massachusetts Institute of Technology, Massachusetts, 1998.
- <sup>10</sup> Hagelaar G. J. M., Bareilles J., Garrigues L., and Boeuf J. P., "Role of anomalous electron transport in a stationary plasma thruster simulation", *J. Appl. Phys.*, Vol. 93, No. 1, pp. 67-75, 2003.
- <sup>11</sup> Parra F.I., Ahedo E., Fife J.M., Martinez-Sanchez M., "A two-dimensional hybrid model of the Hall thruster discharge", *J. Appl. Phys.*, Vol. 100, No. 023304, 2006.
- <sup>12</sup> Janes G.S., Lowder R.S., "Anomalous electron diffusion and ion acceleration in a low-density plasma", *Phys. Fluids*, Vol. 9, No. 6, pp. 115-1123, 1966.
- <sup>13</sup> Litvak A. A., Raitses Y., and Fisch N. J., "Experimental studies of high-frequency azimuthal waves in Hall thrusters", *Phys. Plasmas*, Vol. 11, No. 4, pp. 1701-1705, 2004.
- <sup>14</sup> Lazurenko A., Vial V., Prioul M., and Bouchoule A., "Experimental investigation of high-frequency drifting perturbations in Hall thrusters", *Phys. Plasmas*, Vol. 12, No. 013501, 2005.
- <sup>15</sup> N.B. Meezan, W.A. Hargus, Jr. and M.A. Cappelli, "Anomalous electron mobility in a coaxial Hall discharge plasma", *Phys.Rev. E*, Vol. 63, No. 026410, 2001.
- <sup>16</sup> J.C. Adam, A. Heron, G.Laval, "Study of Stationary plasma thrusters using two-dimensional fully kinetic simulations", *Phys. Plasmas*, Vol. 11, No. 1, pp. 295-305, 2004.
- <sup>17</sup> Hagelaar G.J.M., Bareilles J., Garrigues L., and Boeuf J.P., "Two-dimensional Model of a Stationary Plasma Thruster", *J. Appl. Phys.*, Vol. 91, No. 9, pp. 5592-5598, 2002.
- <sup>18</sup> Hagelaar G.J.M., "Modelling electron transport in magnetized low-temperature discharge plasmas", *Plasma Sources Sci. Technol.*, Vol. 16, S57-S66, 2007.
- <sup>19</sup> D. Meeker, FEMM version 3.1, <http://femm.berlios.de>, 2002.
- <sup>20</sup> Garrigues L., Pérot C., Gascon N., Béchu S., "Characteristics of the SPT100-ML Comparisons Between Experiments and Models", International Electric Propulsion Conf., IEPC Paper, 1999.
- <sup>21</sup> A. Ducrocq, J.C. Adam, A. Heron, and G. Laval, "High-frequency electron drift instability in the cross-field configuration of Hall thrusters", *Phys. Plasmas*, Vol. 13, No. 102111, 2006.
- <sup>22</sup> C.K. Birdsall and A.B. Langdon, "*Plasma physics via computer simulation*", edited by Adam Hilger, IOP Publishing, Philadelphia, USA, 1991.
- <sup>23</sup> Hockney R.W., Eastwood, J.W., "*Computer simulation using particles*", edited by Adam Hilger, IOP Publishing, Bristol, UK, 1988.
- <sup>24</sup> Rax J.M., "*Physique des plasmas*", edited by Dunod, Paris, 2005.